Effect of Surface Chemistry on the Mechanisms and Governing Laws of Friction and Wear

Ling Dai, Viacheslav Sorkin, Yong-Wei Zhang*

*zhangyw@ihpc.a-star.edu.sg

Institute of High Performance Computing, 1 Fusionopolis Way, 16-16 Connexis, 138632, A*STAR, Singapore

Abstract

Recent studies have shown that interface chemistry, that is, the formation and breaking of chemical bonds across contacting interfaces, is closely related to the wear and friction behavior at the nanoscale. In reality, the dangling bond density (DBD) at contacting surfaces can vary greatly. Currently, it remains unclear how friction and wear mechanisms depend on DBDs and whether the Archard's law for wear and Amonton's law for friction are still applicable for contacting surfaces with different DBDs. In this work, we address these issues by studying the wear and friction behavior between two sliding diamond-like carbon surfaces by controlling DBDs via hydrogenation using molecular dynamics simulations. It is found that the chemical bond breaking and remaking across the contacting interface play the key role in determining the friction and wear behavior. During the sliding, a higher DBD leads to more chemical bond formations across the interface, causing stronger wear via either atom or cluster detachments. With the same DBD, a mechanism transition from an atom-by-atom to cluster detachments is observed by increasing the normal load. Remarkably, a fully saturated surface can exhibit a wearless friction. We further show that after necessary modifications, the Archard's law for wear and the Amonton's law for friction may be applicable at the nanoscale. The present work reveals insights into the effect of interface chemistry on the friction and wear, and provides guidelines for effective anti-wear design.

Keyword: friction, wear, NEMS, diamond-like-carbon, molecular dynamics

1. Introduction

Driven by the fast development of nanotechnology, in particular, nano-electromechanical systems (NEMs), friction and wear at the nanoscale are becoming critical issues, and thus drawing great research attention[1-3]. It has been widely accepted that at the nanoscale, the friction forces may interrupt normal performance of NEMs since these forces can reach levels that are comparable to the driving forces[1, 4]. Furthermore, wear induced by friction forces can also damage individual components and thus significantly reduce the lifetime of these systems. Clearly, it is both important and necessary to understand and further quantify the friction and wear behavior at the nanoscale.

Due to the developments and applications of characterization tools, such as Atomic Force Microscopy (AFM)[5] and Lateral Force Microscopy (LFM)[6], many studies have been performed on friction and wear mechanisms at the nanoscale.[6-11] For example, Chung et al.[7] investigated nanoscale sliding using diamond-like carbon (DLC), and characterized wear via AFM. It was found that debris derived from plastic material flow along the sliding track, were able to form agglomerated particles, a phenomenon similar to the macroscopic behavior. Meanwhile, Bhaskaran et al.[8] demonstrated that wear via an atom-by-atom attrition mechanism was also achievable for DLC. Bhushan and Kwak[9] further showed that wear can be strongly related to the combined effect of surface deformation and chemical reaction between contacting surfaces. Surprisingly, such combined effect was also suggested to even dominate the friction forces under wearless sliding[6]. Clearly, these diversified observations suggest the complexity of friction and wear behavior at the nanoscale and also point out the limitation of current experimental characterization techniques due to their inability in precisely manipulating nanoscale samples and directly visualizing contacting interfaces.[11]

Besides friction and wear mechanisms, laws that govern the friction and wear at the nanoscale are also controversial. For example, Archard's law, i.e. $M=k\boldsymbol{F}_z d$, where M the mass of wear (wear-off), $\boldsymbol{F}_z$ is the normal loading force, d is the sliding distance and k is the coefficient, has been well proved to govern the wear behavior for macroscale sliding. Sha et al.[10] claimed that Archard's law was still applicable to the nano-sized cluster wearing in their large-scale MD work. Bhaskaran et al.[8], however, showed that the

wear of a sharp tip was by an atom-by-atom attrition mechanism, and deviation from Archard's law after a certain sliding distance[8] was observed in their experiments. Similarly, the linear Amonton's law, i.e. $\boldsymbol{F_x}=\mu \boldsymbol{F_z}$, where $\boldsymbol{F_x}$ is the friction force, $\boldsymbol{F_z}$ is the normal loading force, and μ is the coefficient of friction, was found to be inapplicable at the nanoscale since the relation between $\boldsymbol{F_x}$ and $\boldsymbol{F_z}$ became nonlinear[11]. At the nanoscale, the effect of interfacial adhesion on the friction was found to be no longer negligible[12]. Modifications by including the interfacial adhesion were suggested[13-15]. In particular, the simple and elegant JKR theory[13] was modified to describe the frictional behavior at the nanoscale[16-17]. It is noted that controversies remain regarding whether the friction behavior at the nanoscale still follows the Amonton's law, owing to the effects of surface roughness[18], contact geometry[19], material compatibility[20], etc.

Recent studies have shown that interface chemistry, that is, the chemical bonds formed or broken across contacting interfaces, is closely related to wear and friction behavior. For example, Gao et al.[21] performed MD simulations to study the interfacial friction between two DLC coating films, and found that chemical reactions across the interface controlled the interfacial adhesion and friction behavior. A high surface saturation by hydrogenation or a further separation of two contacting films could effectively reduce the friction force. In particular, an ultra-low friction force was able to achieve with film surfaces being nearly fully saturated, and thus it was the surface atomic structure rather than the thickness of the amorphous film that dictated the friction properties. Later, Harrison et al.[22] reported that the chemical bond formation and breakage at the two DLC-based film surfaces could reach a stable state and the interfacial friction force could also exhibit a convergence trend after a certain sliding distance, signifying the important effect of chemical reactions on friction mechanics. A recent study on the atomic scale wear using both experiments and MD simulations[23] showed that the rate of atomic wear and the contact stress at DLC surfaces were strongly dependent on the rate of interfacial chemical reactions. Furthermore, Schall et al.[24] analyzed the effect of dangling bond saturation via hydrogenation and showed that the bond formation and breaking at the counterfaces triggered atomic wear and mass transfer across the interface. The debris layer formation and the friction and wear reduction via surface hydrogenation were also

studied by using various means, such as first-principle calculations, MD simulations and experiments[25-28]. These studies consistently showed that the surface chemistry at DLC-based film surfaces controlled the chemical reactions across the counterfaces, which in turn determined the friction and wear behavior there. In addition, Dag and Ciraci[29] performed first-principles calculations and showed that the hydrogen atoms (H-atoms) on the DLC surfaces can turn the interfacial interactions from attractive to repulsive so as to increase the separation between the contacting bodies, and therefore reduce the friction force. Clearly, these studies highlight the importance of interface chemistry in influencing the friction and wear mechanisms.

External loading is another important factor that can affect friction and wear. It is well-known that at the nanoscale, the counterfaces make contacts only at discrete regions. As a result, only a small number of atoms with dangling bonds are able to locate closely enough to form chemical bonds. A large external normal load can flatten the counterfaces to create new dangling bonds and also to bring distant dangling atoms together to form new chemical bonds. These newly formed chemical bonds are likely to cause a higher friction force and a stronger wear. The above analysis and discussion highlight the importance of interface chemistry and its coupling with mechanical loading in affecting the wear and friction mechanisms and behavior.

In reality, the coverage and distribution of dangling bonds at contacting surfaces can vary significantly. Then interesting questions arise: How are friction and wear mechanisms dependent on surface dangling bond density (DBD)? Are the Archard's law and Amonton's law applicable to contacting surfaces with different DBDs? Clearly answers to these questions are not only of great scientific interest, but also of enormous technological impact on the development of NEMS devices. In this work, we study the wear and friction behavior between two sliding DLC surfaces by varying the normal loading and surface DBDs using molecular dynamics simulations. Our intent is to answer the aforementioned questions.

2. Model

Our MD simulations were carried out using LAMMPS package[30] with a time step of 0.2fs, and the modified Tersoff potential[31] was used to compute the atomic interactions at a cut-off distance (r_{cut}) of 1.2nm. We constructed an amorphous DLC structure based on the procedure developed by Sha et al.[31] to form the DLC films and tips. The DLC structure is comprised of 80.2% sp^3, 19.2% sp^2, and 0.6% sp types of C-C bonds. The mass density and Young's modulus of the constructed structure were shown to be consistent with experimental results[31]. In addition, this DLC structure was also successfully applied to study the wear mechanism and law at the nanoscale[10]. As shown in Fig.1(a), the DLC substrate (SUB) had dimensions of 30, 6 and 3nm along the X, Y and Z axis, respectively. Periodic boundary conditions were applied at the lateral XY plane. Along the Z axis, the atoms within 0.5nm from the bottom were fixed, and those within 0.5nm above the fixed layer were set as a thermostat, in which the atomic velocities were scaled every 20fs to keep the temperature at 300K. The DLC sliding tip was constructed as a cylinder with its bottom end capped by a hemisphere (Fig.1(a)). The length of the cylinder is 4nm and its radius is 2nm. The atoms within 1nm from the top of the cylinder were constrained as a single rigid block (RIG, Fig.1(a)). The tip was initially positioned at 1.2nm (r_{cut}) above the film substrate surface to avoid initial interaction between the tip and SUB. A constant normal load ($\boldsymbol{F_z}$) was applied to the rigid block so as to push the tip downwards towards the substrate surface. Note that the force $\boldsymbol{F_z}$ was uniformly distributed among all the atoms in the rigid block. After equilibration, a constant velocity of 20m/s was assigned to the rigid block. The tip was set to slide for a total distance of 20nm.

Since both the tip and SUB are pure DLC, there are dangling bonds present in the C-atoms at both counterfaces. To control the DBD at these surfaces, we saturated these surface dangling bonds by hydrogenation. We chose five different levels of hydrogenation density (%H), that is, 0%H (Model-O), 25%H (Model-I), 50%H (Model-II), 75%H (Model-III) and 100%H (Model-IV), for both tip and SUB surfaces. Hence, Model-O was free of H-atoms while Model-IV was free of dangling bonds on the surfaces. For each model, we applied different values of $\boldsymbol{F_z}$, from the lowest 0.12nN to the highest 12nN, to study the load effect.

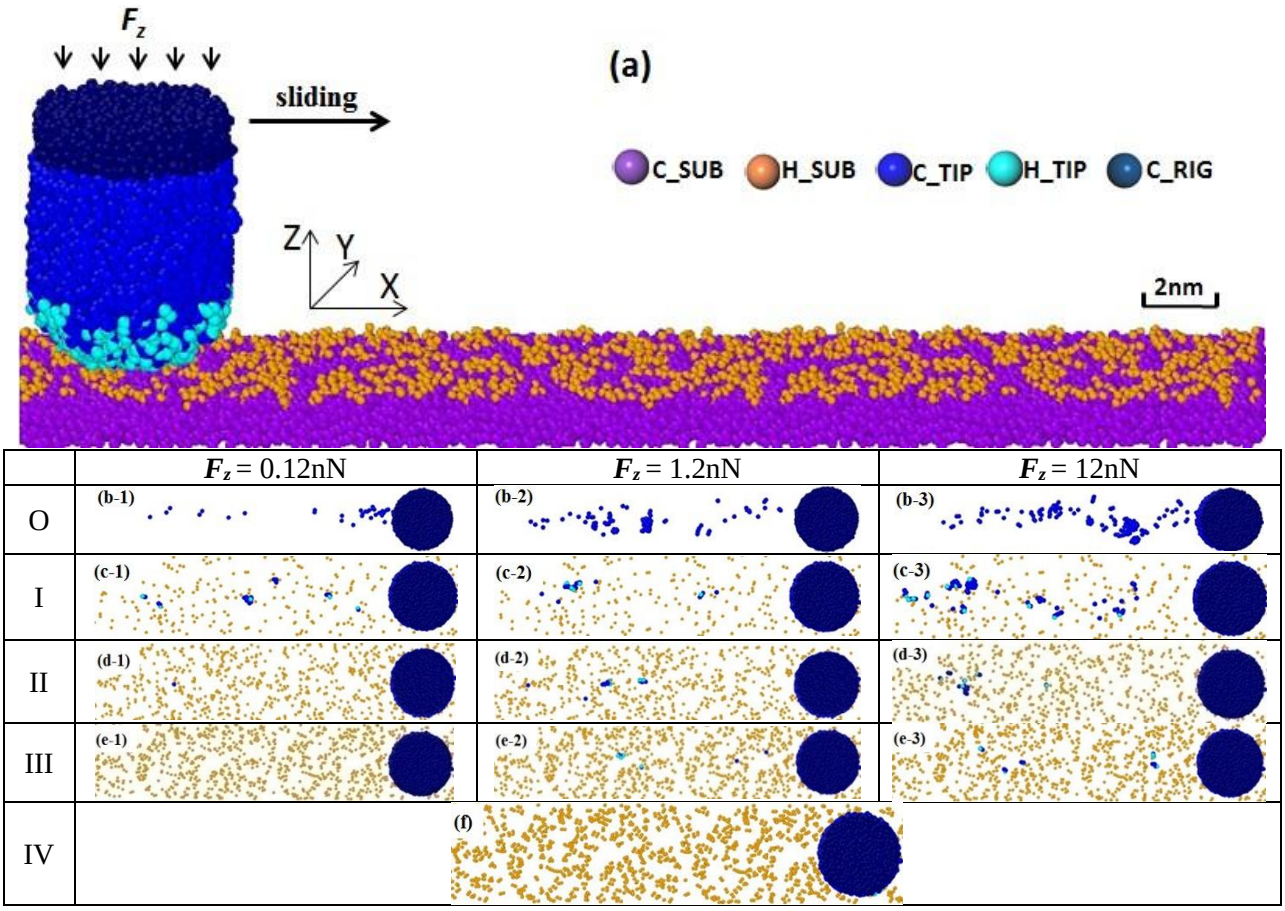

Fig.1. (a) Three-dimensional view of the simulation setup for the DLC substrate and sliding tip, where the atoms within different groups are differentiated by colors. The atoms within the rigid block of the tip were applied with a normal load (F_z) as well as assigned a sliding velocity of 20m/s.
(b)-(e) Top views of (b) Model-O, (c) Model-I, (d) Model-II, and (e) Model-III, after a sliding distance of 20nm under different levels of F_z: 0.12nN for (b-1), (c-1), (d-1) and (e-1), 1.2nN for (b-2), (c-2), (d-2) and (e-2), and 12nN for (b-3), (c-3), (d-3) and (e-3), where the C-atoms in SUB were not shown for clarity.
(f) Top views of Model-IV after a sliding distance of 20nm, showing a wearless friction at F_z=12nN, where the C-atoms in SUB were not shown for clarity.

3. Results and Discussions

First of all, we examined the atomic motions along the contacting interface between the tip and SUB for Model-O. During the sliding, it was observed that there was a strong tendency for the atoms at the tip and SUB surfaces to transfer across the interface. Such transfer of atoms was made possible by the chemical bonds formed at one position and then broken at another position across the contact interface. When F_z was small, for example, 0.12nN, the wear-off atoms from the tip were mostly in the form of

isolated atoms as shown in Fig.1(b-1). However, when the loading level was increased, (for example, at $\boldsymbol{F_z}$=1.2nN, Fig.1(b-2)), larger size wear-off clusters started to appear. When the loading level was further increased, (for example, at $\boldsymbol{F_z}$=12nN, Fig.1(b-3)), wear-off clusters became more prevalent and their sizes became even larger. The observed strong wear at the amorphous DLC surfaces is consistent with previous studies with the same DLC structure[10].

For Model-I with a 25%H coverage on the surfaces, the wear-off level was obviously lower than that for Model-O, indicating that hydrogenation coverage was able to reduce the wear rate. The mean wear-off cluster size was also observed to increase with the increase of $\boldsymbol{F_z}$ from isolated atoms to increasingly larger clusters (Fig.1(c-1) for 0.12 nN, Fig.1(c-2) for 1.2 nN, and Fig.1(c-3) for 12nN). Our study here shows that hydrogenation can effectively saturate the dangling bonds, and thus significantly reduce the chemical reactivity of C atoms at the a-DLC sample surfaces. This observation is consistent with previous experimental and simulation studies[21-22, 24, 29].

It should be noted that only C atoms with dangling bonds are able to form interfacial chemical bonds (ICBs), and depending on the level of %H, H atoms are able to partially or completely saturate the dangling bonds in the surface C atoms, thus reducing the possibility for forming ICBs and also shielding the dangling bonds in the carbon atoms below them from forming ICBs. This is the physical origin why surface hydrogenation is able to reduce wear rate.

In our simulations, however, we did not observe any bond breaking between H and C atoms, indicating that the wear-off is dictated by C-C bond breakage. In fact, we find that wear-off debris is either in the form of individual C-atoms, or debris with pure C-atoms, or debris containing C-H groups. When the tip and substrate surfaces are partially hydrogenated, the unsaturated dangling bonds across the interface between the two surfaces can react to form ICBs. Such ICBs can cause the detachment of debris, in which some of C atoms may be bonded with H atoms. As a consequence, C-H groups may be found in wear debris. When the tip and substrate surfaces are fully hydrogenated, both surfaces are free of dangling bonds. In such scenario, a large indentation force is needed to deform the tip and substrate surfaces plastically, that is, the surfaces are compressed to such an extent that dangling bonds in the C-atoms

behind the C-H groups become exposed. These exposed dangling bonds across the interface between the tip and substrate surfaces can thus form ICBs. Once ICBs are formed, wear-off becomes inevitable. Since some of C atoms in the debris may be bonded with H atoms, thus C-H groups may be found in wear debris.

With a further increase in hydrogenation coverage %H, the wear level was further decreased for the same loading level. This can be clearly seen from the simulation results as shown in Model-II and Model-III. For example, the wear-off became barely observable at $\boldsymbol{F_z}$ = 0.12nN for Model-II as shown in Fig.1(d-1) and Model-III as shown in Fig.1(e-1). At $\boldsymbol{F_z}$=1.2nN, the wear took the form of scarcely distributed atoms (Fig.1(d-2) for Model-II and Fig.1(e-2) for Model-III). Only at $\boldsymbol{F_z}$=12nN, the wear became dominated by the cluster detachment mechanism (Fig.1(d-3) for Model-II and Fig.1(e-3) for Model-III). Interestingly, when the surface hydrogenation coverage reached the full saturation as in Model-IV, the sliding became wearless even at the loading level of $\boldsymbol{F_z}$ =12nN (Fig.1(f)).

The above simulation results clearly show that with the decreased hydrogenation coverage and/or the increased loading level, the wear rate increases. For the complete surface hydrogenation, however, the sliding becomes wearless within the scale of all applied normal loadings studied here. Clearly, for atoms to wear off, they need to form interfacial C-C bonds (ICBs) across the contacting interface between the tip and SUB. Therefore, we examined the quantity of ICBs during the sliding process. The time-averaged ICB quantities for each model under different values of $\boldsymbol{F_z}$ are plotted in Fig.2. It is seen clearly that more ICBs were formed when there were more DBDs at the initial counterfaces. When a higher $\boldsymbol{F_z}$ was applied, it brought the two counterfaces closer, enabling the formation of more ICBs across the two counterfaces. During the sliding, the connections via ICBs would eventually break, triggering the wear-off. However, we note that there could be the mass transfer across the interface, which included the multiple cycles of ICB formation and breakage before the final wear-off. Remarkably, when the counterfaces were fully saturated (as in the case of Model-IV) and when the loading was unable to create new surface dangling bonds during sliding, there would be no ICBs formed, and thus no wear.

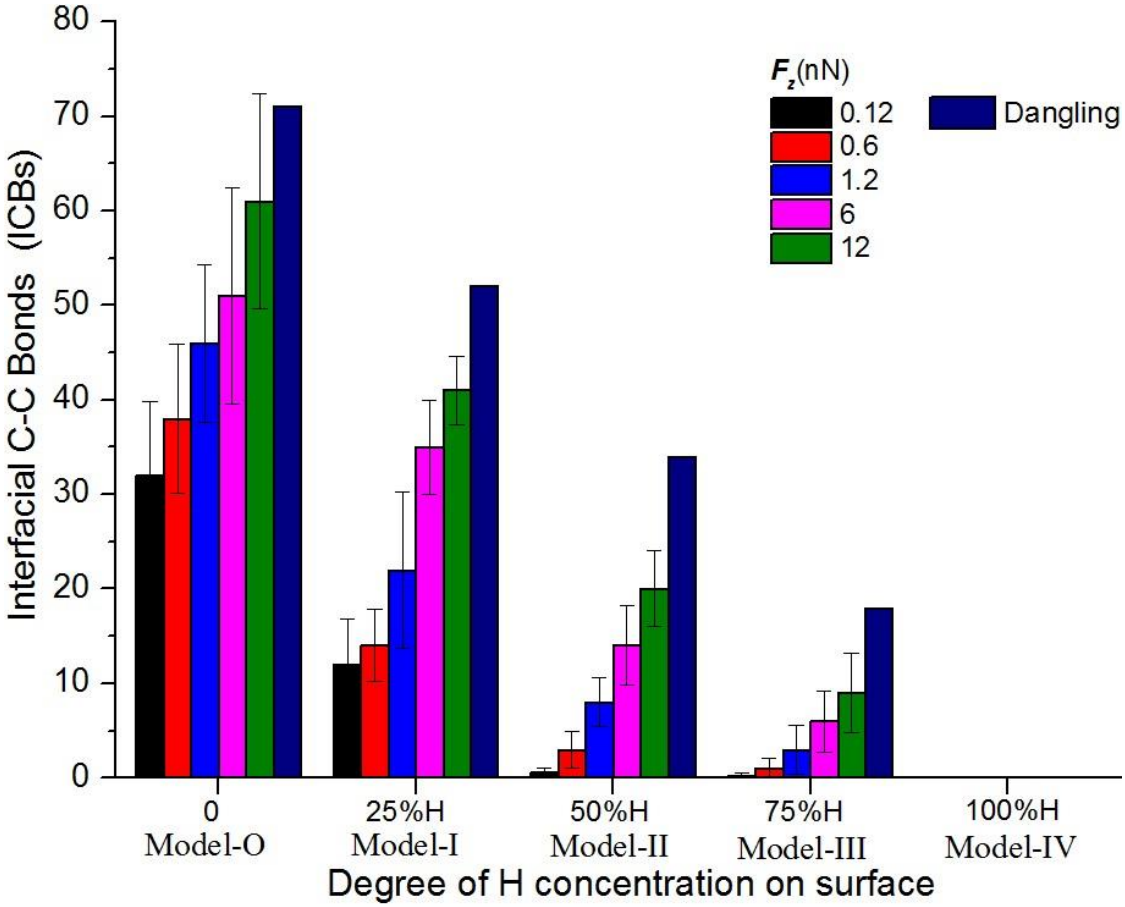

Fig.2. Time-averaged ICBs during the sliding distance of 20nm, together with the number of initial dangling bonds on the tip surface at different hydrogenation levels (%H) and under different values of $\boldsymbol{F_z}$. The error bars are also given.

Besides the quantity of ICBs, the loading level $\boldsymbol{F_z}$ could also profoundly affect the behavior of individual ICBs. In our simulations, we found that the surfaces of the counterfaces are noticeably undulated. The maximum range of the surface roughness (from the most protrusion to the most concave point) could reach 0.6nm, which was significantly larger than the standard bond length of ICBs (~ 0.154nm). Therefore, in general, ICBs could be only formed at the protruding regions where the two counterfaces were located in close proximity. Thus, under a low $\boldsymbol{F_z}$, few ICBs were able to form across the interface. Case-I in Fig.3(a) illustrates such scenario: Among the three atoms located at the tip surface, atom-B was originally bonded with atom-A and atom-C. The atom-A was connected with a SUB atom by forming an ICB (bond-α). During sliding, atom-A detached from the tip via bond breaking with atom-B, rather than via breaking of the ICB, bond-α, causing the wear-off of atom-A. Since other atoms in the tip,

such as atom-C, were widely separated from atom-A, it was impossible for atom-A to re-make ICB, and thus atom-A maintained its wear-off status afterwards.

Meanwhile, a higher $\boldsymbol{F_z}$ was able to flatten the counterfaces and bring more atoms at the tip surface (like the atom-C) closer to SUB, and thus the possibility of forming ICBs was enhanced. Case-II in Fig.3(a) illustrates such scenario: When atom-A was detached from the tip, a new bond (bond-β), which was located near the ICB (bond-α), could be formed between atom-A and atom-C. This led to the formation of an atomic chain. Subsequently, this chain could fall apart and detach from the tip in different ways as illustrated in Fig-3(a). One possible way is that the chain could detach from the tip (Case-II-a), leading to a cluster wear-off of atom-A and atom-C. Another possible way is that the bond-β (Case-II-b) could be broken, in which case atom-A became wear-off again. Alternatively, the bond-α could be broken (Case-II-c), in which case atom-A was re-attached to the tip and there was no wear-off. Thus, in Case-I, the wear-off was only one-time detachment process, while in Case-II, wear-off proceeded through multiple cycles of attachment-detachment before the final detachment. We observed that the wear-off chains (Case-II-a) or atoms (Case-II-b) could re-bond to other atoms with dangling bonds, and repeat the attachment-detachment cycles of the wear-off process. As shown in Fig.3(b), those highlighted C-atoms originally located along the tip surface (Panel-(1)) gradually transported backwards (Panel-(2)), causing mass aggregation at the rear side of the contact interface (Panel-(3)) to form a cluster, which then detached from the tip, forming the wear-off cluster on the substrate surface (Panel-(4)). Such material transfer was also observed in previous studies[10, 23-24].

Based on the above analysis, we concluded that the wear-off was determined by the quantity and distribution of ICBs, which were substantially influenced by %H and $\boldsymbol{F_z}$. Our MD simulations indicate that %H on the counterfaces is the potential source for ICBs. In model-O, on the undulated rough counterfaces, some ICBs could form naturally between the dangling bonds at the tip and SUB surfaces even under a very low $\boldsymbol{F_z}$. Comparatively, in other models, the number of the ICBs decreased dramatically with the increase in surface saturation. For example, in Model-II, ICBs almost disappeared when %H

reached 50%. Meanwhile, under a higher load F_z, the counterfaces were brought in closer proximity and deformed more conformably, resulting in more ICBs.

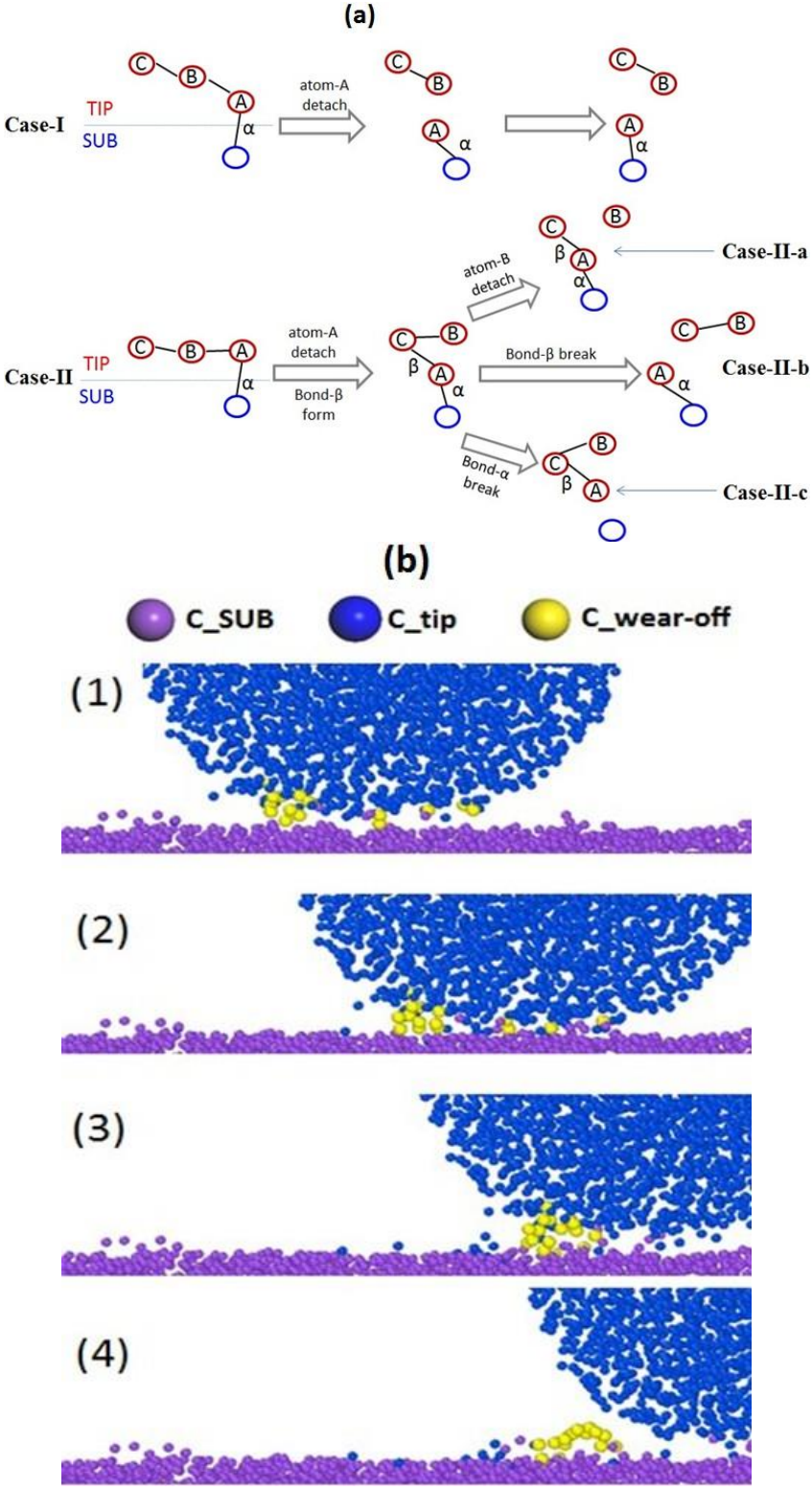

Fig.3.(a) The behavior of wear-off for two cases. Case-I: one-time attachment and detachment, and Case-II: multiple attachment-detachment cycles. The red hollow circles stand for tip atoms and blue hollow circles stand for SUB atoms.
(b) Snapshots showing the formation of a wear-off cluster. (1) Initial atomic positions, (2) Mass transport along the contact interface, (3) Mass aggregation at the trailing end, and (4) detachment of the cluster. The atoms in the wear-off cluster are highlighted in yellow.

Furthermore, $\boldsymbol{F_z}$ also affects the wear-off mechanism. As discussed previously (Fig.3), under a low $\boldsymbol{F_z}$, ICBs were mostly isolatedly distributed along the interface, and one-time detachment process was prevalent, triggering the isolated atom-by-atom attrition mechanism of wear-off. However, under a higher $\boldsymbol{F_z}$, a larger number of wear-off atoms aggregated via multiple cycles of attachment/detachment process, leading to the cluster wear-off mechanism. It is noted that the effects of $\boldsymbol{F_z}$ could persist as long as atoms with dangling bonds were present on the counterfaces. However, for the completely saturated Model-IV with no dangling bonds at the counterfaces, if the applied load was unable to create any new dangling bonds, wear-off was not possible.

The wear-off process occurring at the tip can be regarded as a failure process along the contact interface. Below, we use Model-O as an example to examine the stress state at the contact area. Here we use two methods to define the contact area: 1). the contact area is defined as the lateral area enclosed by the envelope of all the individual ICBs, and 2) the contact area is define as the summation of contact areas of all the individual ICBs. For the latter, the contact area for each ICB is approximately taken as the unit area of the diamond lattice size[32]. Our calculations based on the former definition give the average value of contact area of 0.055nm^2 when $\boldsymbol{F_z}$ =0.12nN, and gradually increase to 2.22nm^2 when $\boldsymbol{F_z}$ increased to 12nN. For the latter definition, the contact area is in the range of 0.038 nm^2 to 1.54 nm^2 under the same range of $\boldsymbol{F_z}$. Thus, the contact stress based on these two definitions is predicted to be in the range of 2.18 to 7.79 GPa, which is on par with previously reported failure strength range of 2.2-8.5 GPa for DLC films[33]. Hence, the failure mechanism based on the cluster detachment is consistent with the failure process at the contact interface based on contact mechanics.

Archard's law, $M = kF_z d$, has been widely used to describe wear at the macroscale. The coefficient k includes the effects of many factors, such as the %H, wear-off mechanism, etc. We present the relation

between M and $\boldsymbol{F_z}$ obtained from all the models in Fig.4(a). It can be seen that within the sliding distance of d=20nm, there are two different wear-off stages (and two values of k, correspondingly). More specifically, there exists a critical normal force of about 1.2nN, which separates these two stages, with a higher k at $\boldsymbol{F_z}$ <1.2nN and a lower k at $\boldsymbol{F_z}$ >1.2nN. We found that when $\boldsymbol{F_z}$ <1.2nN, the wear-off mechanism was manifested by attrition of isolated atoms, and therefore, the number of the wear-off atoms increased steadily with $\boldsymbol{F_z}$. Such atom-by-atom attrition wear has also been reported in previous experimental studies[9, 34-35]. When $\boldsymbol{F_z}$ exceeded 1.2nN, the atoms were able to aggregate along the counterfaces, and the wear proceeded through multiple detachment-attachment cycles. The number of wear-off atoms increased moderately with the increase of $\boldsymbol{F_z}$. We also plotted the number of wear-off atoms as a function of the sliding distance (Fig.4(b)) for the different values of %H under $\boldsymbol{F_z}$=1.2nN, and different values of $\boldsymbol{F_z}$ (for Model-I) (Fig.4(c)). It can be seen that M increased in a fairly linear manner with the sliding distance, consistent with Archard's law. However, it should be noted that there are two distinct normal load-dependent stages, corresponding to two distinct wear mechanisms. Hence, in order to apply Archard's law here, we need to use two different values of k, to include the effect of normal loading $\boldsymbol{F_z}$. Below the critical normal load, there is negligible surface deformation; while above the critical load, plastic deformation leads to enhanced ICB formation at the counterfaces and triggers cluster wear-off mechanism. It was reported previously that the failure of Archard's law was attributed to blunting of a sharp sliding tip.[8, 36] Our study here indicates that this failure could be attributed to the transition of wear mechanism from an isolated atom-by-atom wear of a sharp tip to a cluster-based wear of a blunted tip.

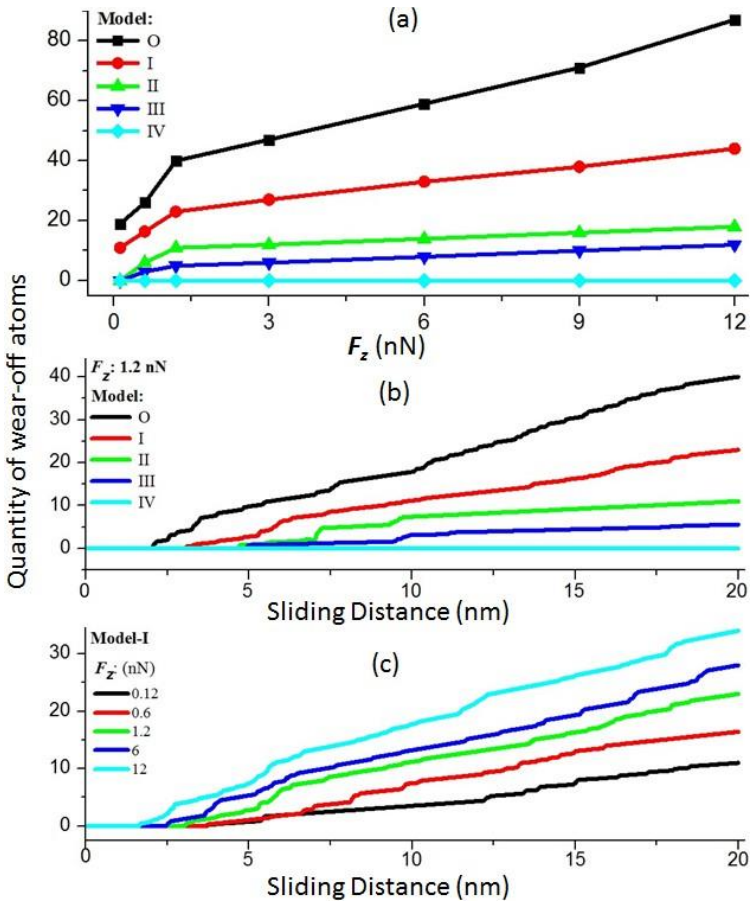

Fig.4. Data plot for the atom quantity of wear-off (a) Total wear after 20nm sliding vs. F_z for different models (b) Time-history for F_z=1.2nN, with different models; (c) Time-history for 25%H Model-I, under different F_z.

In addition to wear, friction is also critical to NEMs performance. This is because, at the nanoscale, chemical interactions across the contacting interface may lead to significant adhesion and thus greatly influence friction behavior[21, 32]. The adhesion force in general can be divided into two parts: the chemical bonding force and the non-chemical bonding force. Apparently, a lower %H is able to result in a stronger chemical bonding force and a higher adhesion strength (Fig.5(a)) due to the larger number of ICBs. Of particular interest is that the completely saturated counterfaces of Model-IV are free of ICBs, and thus the interfacial force is only the non-chemical bonding force. Since the chemical bonding force is much stronger than the non-chemical bonding force, it is expected that interface chemistry dominates the friction and wear behavior at the nanoscale.

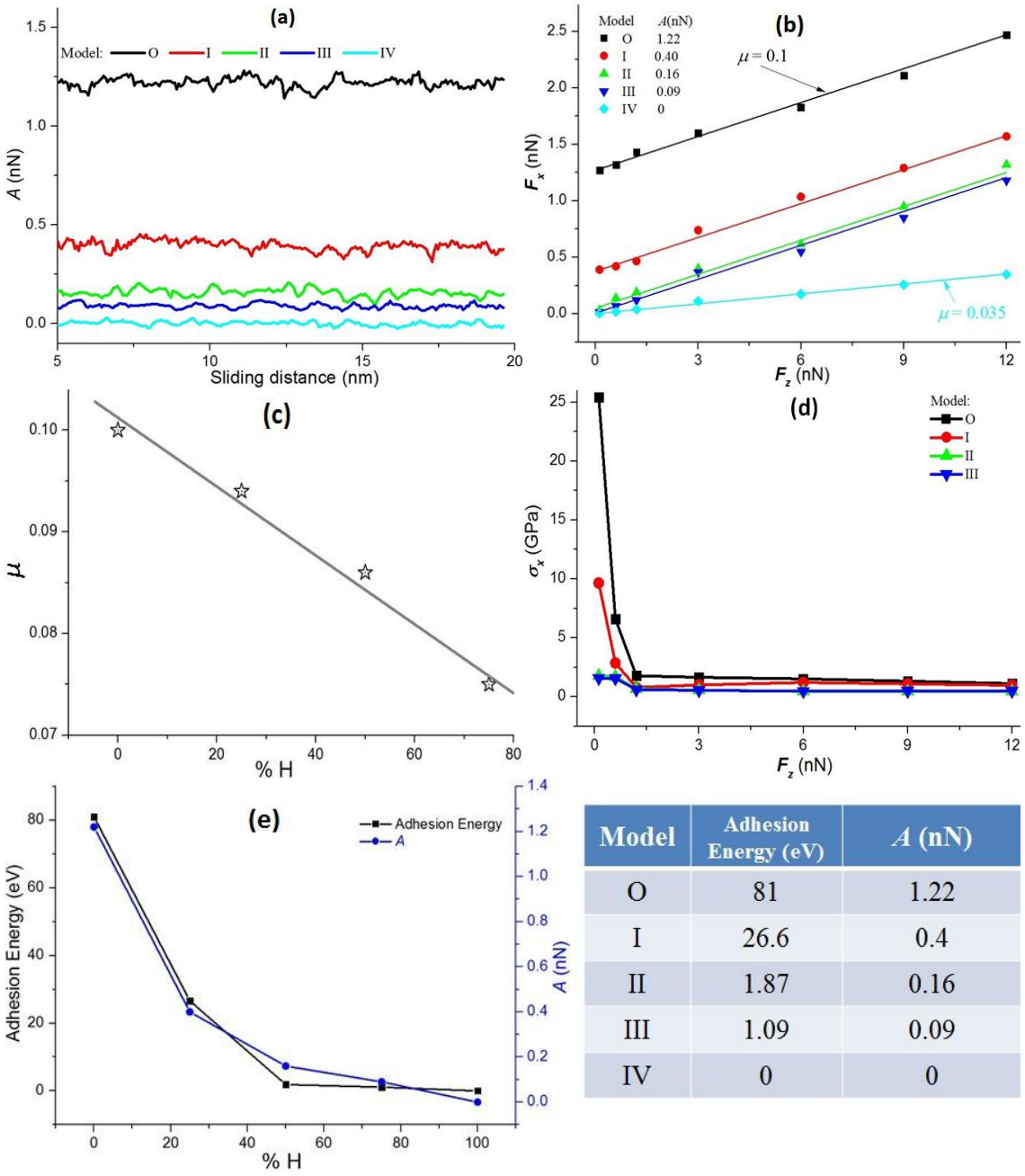

Model	Adhesion Energy (eV)	*A* (nN)
O	81	1.22
I	26.6	0.4
II	1.87	0.16
III	1.09	0.09
IV	0	0

Figure-5. (a) The value of the friction force *A* in the absence of the normal force (F_z=0) as a function of sliding distance for different models.
(b) The total friction force $\boldsymbol{F_x}$ vs. the normal force $\boldsymbol{F_z}$, with linear fitting based on the modified Amonton's law. The values of *A* and μ for each model are listed in the inset.
(c) The linear μ vs. %H relation.
(d) Interfacial shear strength $\boldsymbol{\sigma_x}$ vs. $\boldsymbol{F_z}$.
(e) Interfacial adhesion energy and its associated shear force as a function of %H under $\boldsymbol{F_z}$=0. The computed data for the adhesion energy and *A* were shown in the table at the right side.

In order to consider the adhesion effect, we divide the total friction force into two parts: the friction force associated with the normal force and the friction force in the absence of the normal force. Thus, the

total friction force $\boldsymbol{F_x}$ can be written as $F_x = A + \mu F_z$, a modified Amonton's law, where A is the friction force without the external normal force (that is, $\boldsymbol{F_z}$=0), and μ is the coefficient of friction (COF). The calculated value of A with sliding distance for each model is shown in Fig.5(a). It is seen that the value of A decreases drastically with the increase of %H since the interfacial adhesion is predominantly controlled by chemical bonding force due to the formation of ICBs across the counterfaces. For each model, however, the value of A is approximately constant. The time-averaged $\boldsymbol{F_x}$ as a function of $\boldsymbol{F_z}$ for each model is plotted in Fig.5(b). It is seen that the total friction force $\boldsymbol{F_x}$ increases linearly with increasing the normal force $\boldsymbol{F_z}$. For model-IV with fully saturated counterfaces, the adhesion force is small and thus the COF value is correspondingly small with only μ=0.035. For other models, both A and μ increase with the decrease of %H. In fact, the friction force is linearly dependent on %H. As shown in Fig.5(c), μ decreases linearly with %H as long as ICBs are present at the contacting interface. Thus, the modified Amonton's law, which includes the adhesion effect, is able to describe the simulation results. It should be noted that different values of %H for different models are reflected in the different values of A and μ, as shown in Fig.5(c).

The Bowden and Tabor's theory (BT theory)[37] states that the asperity counterface deformed plastically and the interfacial stress component corresponds to the shear strength of the material. To check if the wear process follows the BT theory, we calculate the interfacial shear strength from our simulations. To do so, we need to define the real contact area, A_{ctc}, which is taken as a summation of areas of all individual ICBs. Then the shear strength $\boldsymbol{\sigma_x}$ can be obtained by $\boldsymbol{F_x}/A_{ctc}$. The calculated results against $\boldsymbol{F_z}$ are plotted in Fig.5(d). It is seen that there are two distinctive regimes for the variation of $\boldsymbol{\sigma_x}$ with $\boldsymbol{F_z}$: Below $\boldsymbol{F_z}$=1.2, the shear strength decreases with increasing $\boldsymbol{F_z}$, while above which, the shear strength is more or less a constant. Interestingly, the two regimes match exactly with the two distinctive wear-off regimes: the atom-by-atom attrition and the cluster detachment. It is seen that for the latter regime, the shear strength is about 1.8~2.2 GPa, which is on par with the lower bound of previously reported failure strength range of 2.2-8.5 GPa for DLC films.[26] For the former, however, the shear strength varies significantly, depending on both %H and the loading levels, which may explain the large variation in

experimental measurement for the shear strength.[26] Hence, we conclude that the wear-off through the atom-by-atom attrition does not follow the BT theory, while wear-off through cluster detachment does. The underlying reason for this is likely due to the fact that for the former, wear-off is only through sporadic bond breakage, while for the latter, the counterface experiences continuous plastic deformation during sliding. Since one of the assumptions in the BT theory requires that the asperity counterface should deform plastically. Clearly, the latter satisfies this assumption while the former does not.

For each model, we also measured the interfacial adhesion energy under $\boldsymbol{F_z}$=0. The calculated results together with the values of *A* as a function of %H are shown in Fig.5(e). It is seen that the adhesion energy and the value of *A* are strongly correlated and show the similar trend. Evidently, a lower %H coverage leads to a higher adhesion via forming more ICBs, and thereby a higher shear force during sliding.

4. Conclusion

Through MD simulations, we show that the wear and friction behavior between a DLC tip and DLC film with different surface hydrogenated coverages is strongly correlated with the ICBs across the contacting interface, which are dictated by two main factors, %H and $\boldsymbol{F_z}$. With a lower %H, there are more C-atoms with dangling bonds along the counterfaces, facilitating the formation of more ICBs. Meanwhile, a higher $\boldsymbol{F_z}$ is able to press the two counterfaces closer to each other, so that more C-atoms with dangling bonds at the counterfaces are able to form ICBs. With more ICBs, more atomic detachment will take place, resulting in more wear-off. Furthermore, with the increase of $\boldsymbol{F_z}$, there is a wear-off transition from isolated atom to cluster detachments. Such mechanism transition gives rise to two wear-off stages and exhibits a bilinear relationship between the amount of wear-off and the normal force $\boldsymbol{F_z}$. Interestingly, the wear-off through the atom-by-atom attrition does not follow the BT theory, while wear-off through cluster detachment does. We also find that ICBs determine the friction behavior. With a lower %H, more ICBs are able to form, giving rise to a stronger adhesion force when $\boldsymbol{F_z}$=0. By excluding the friction force due to the adhesion, we find that the friction force was proportional to the normal load,

consistent with the modified Amonton's law. To reduce wear at sliding interfaces, it is effective by saturating the dangling atoms on the counterfaces and limiting the normal load to a low value. Importantly, when the counterfaces are fully saturated, the sliding process becomes wearless. Such anti-wear design strategy could effectively minimize or even eliminate wear in NEMS and depth-sensing instruments, such as AFM and LFM.

Acknowledgement:

The authors are grateful for the financial support from A*STAR, Singapore and the use of supercomputing facilities at ACRC, Singapore.

1. Kim, S. H.; Asay, D. B.; Dugger, M. T., Nanotribology and MEMS. *Nanotoday* **2007,** *2*, 22.
2. Bhushan, B., Nanotribology and Nanomechanics of MEMS/NEMS and BioMEMS/BioNEMS Materials and Devices. *Microelectron. Eng.* **2007,** *84*, 387-412.
3. Ozaydin-Ince, G.; Coclite, A. M.; Gleason, K. K., CVD of Polymeric Thin Films: Applications in Sensors, Biotechnology, Microelectronics/Organic Electronics, Microfluidics, MEMS, Composites and Membranes. *Rep. Prog. Phys.* **2012,** *70*, 016501.
4. Maboudian, R.; Howe, R. T., Critical Review: Adhesion in Surface Micromechanical Structures. *J. Vac. Sci. Technol. B* **1997,** *15*, 1-20.
5. Bhushan, B., Nanotribology, Nanomechanics and Nanomaterials Characterization. *Philos. Trans. R. Soc., A* **2008,** *366*, 1351-1381.
6. Achanta, S.; Drees, D.; Celis, J. P., Friction from Nano to Macroforce Scales Analyzed by Single and Multiple-asperity Contact Approaches. *Surf. Coat. Technol.* **2008,** *202*, 6127-6135.
7. Chung, K. H.; Kim, D. E., Fundamental Investigation of Micro Wear Rate Using an Atomic Force Microscope. *Tribol. Lett.* **2003,** *15*, 135-144.
8. Bhaskaran, H.; Gotsmann, B.; Sebastian, A.; Drechsler, U.; Lantz, M. A.; Despont, M.; Jaroenapibal, P.; Carpick, R. W.; Chen, Y.; Sridharan, K., Ultralow Nanoscale Wear Through Atom-by-atom Attrition in Silicon-containing diamond-like Carbon. *Nat. Nanotechnol.* **2010,** *5*, 181-185.
9. Bhushan, B.; Kwak, K. J., Velocity Dependence of Nanoscale Wear in Atomic Force Microscopy. *Appl. Phys. Lett.* **2007,** *91*, 163113.
10. Sha, Z. D.; Sorkin, V.; Branicio, P. S.; Pei, Q. X.; Zhang, Y. W.; Srolovitz, D. J., Large-scale Molecular Dynamics Simulations of Wear in Diamond-like Carbon at the Nanoscale. *Appl. Phys. Lett.* **2013,** *103*, 073118.
11. Harrison, J. A.; Gao, G. T.; Schall, J. D.; Knippenberg, M. T.; Mikulski, P. T., Friction between Solids. *Philos. Trans. R. Soc., A* **2008,** *366*, 1469-1495.
12. Zappone, B.; Rosenberg, K. H.; Istaelachvili, J., Role of Nanometer Roughness on the adhesion and Friction of a Rough Polymer Surface and a Molecularly Smooth Mica Surface. *Tribol. Lett.* **2007,** *26*, 191.
13. Johnson, K. L.; Kendall, K.; Roberts, A. D., Surface Energy and the contact of Elastic Solids. *Philos. Trans. R. Soc., A* **1971,** *324*, 301-313.

14. Tabor, D., Surface Forces and Surface Interactions. *J. Colloid Interface Sci.* **1977,** *58*, 2-13.
15. Maugis, D., Adhesion of Spheres: The JKR-DMT Transition Using a Dugdale Model. *J. Colloid Interface Sci.* **1992,** *150*, 243-269.
16. Johnson, K. L.; Sridhar, I., Adhesion Between a Spherical Indenter and an Elastic Solid with a Compliant Elastic Coating. *J. Phys. D: Appl. Phys.* **2001,** *34*, 683-689.
17. Szlufarska, I.; Chandross, M.; Carpick, R. W., Recent Advances in Single-asperity Nanotribology. *J. Phys. D: Appl. Phys.* **2008,** *41*, 123001-123039.
18. Jacobs, T. D. B.; Ryan, K. E.; Keating, P. L.; Grierson, D. S.; Lefever, J. A.; Turner, K. T.; Harrison, J. A.; Carpick, R. W., The Effect of Atomic-Scale Roughness on the Adhesion of Nanoscale Asperities: A Combined Simulation and Experimental Investigation. *Tribol. Lett.* **2013,** *50*, 81-93.
19. Luan, B.; Robbins, M. O., Contact of Single Asperities with Varying Adhesion: Comparing Continuum Mechanics to Stomistic Simulations. *Phys. Rev. E* **2006,** *74*, 026111.
20. Muser, M. H., Nature of Mechanical Instabilities and Their Effect on Kinetic Friction. *Phys. Rev. Lett.* **2002,** *89*, 224301.
21. Gao, G. T.; Mikulski, P. T.; Harrison, J. A., Molecular-Scale Tribology of Amorphous Carbon Coatings: Effects of Film Thickness, Adhesion, and Long-Range Interactions. *J. Am. Chem. Soc.* **2002,** *124*, 7202-7209.
22. Harrison, J. A.; Schall, J. D.; Knippenberg, M. T.; Gao, G. T.; Mikulski, P. T., Elucidating Atomic-scale Friction using Molecular Dynamics and Specialized Analysis Techniques. *J. Phys.: Condens. Matter* **2008,** *20*, 354009.
23. Vahdat, V.; Ryan, K. E.; Keating, P. L.; Jiang, Y. J.; Adiga, S. P.; Schall, J. D.; Turner, K. T.; Harrison, J. A.; Carpick, R. W., Atomic-Scale Wear of Amorphous Hydrogenated Carbon during Intermittent Contact: A Combined Study Using Experiment, Simulation, and Theory. *ACS Nano* **2014,** *8*, 7027-7040.
24. Schall, J. D.; Gao, G. T.; Harrison, J. A., Effects of Adhesion and Transfer Film Formation on the Tribology of Self-Mated DLC Contacts. *J. Phys. Chem. C* **2010,** *114*, 5321-5330.
25. Pastewka, L.; Moser, S.; Moseler, M.; Blug, B.; S.Meier; Hollstein, T.; Gumbsch, P., The Running-in of Amorphous Hydrocarbon Tribocoatings: a Comparison Between Experiment and Molecular Dynamics Simulations. *Int. J. Mater. Res.* **2008,** *99*, 1136-1143.
26. Pastewka, L.; Moser, S.; Moseler, M., Atomistic Insights into the Running-in, Lubrication, and Failure of Hydrogenated Diamond-Like Carbon Coatings. *Tribol. Lett.* **2010,** *39*, 49.
27. Moras, G.; Pastewka, L.; Gumbsch, P.; Moseler, M., Formation and Oxidation of Linear Carbon Chains and Their Role in the Wear of Carbon Materials. *Tribol. Lett.* **2011,** *44*, 355-365.
28. Kunze, T.; Posselt, M.; Gemming, S.; Seifert, F.; Konicek, A. R.; Carpick, R. W.; Pastewka, L.; Moseler, M., Wear, Plasticity, and Rehybridization in Tetrahedral Amorphous Carbon. *Tribol. Lett.* **2014,** *53*, 119-126.
29. Dag, S.; Ciraci, S., Atomic Scale Study of Superlow Friction between Hydrogenated Diamond Surfaces. *Phys. Rev. B* **2004,** *70*, 241401(R).
30. Plimpton, S. J., Fast Parallel Algorithms for Short-Range Molecular Dynamics. *J. Comput. Phys.* **1995,** *117*, 1-19.
31. Sha, Z. D.; Branicio, P. S.; Pei, Q. X.; Sorkin, V.; Zhang, Y. W., A Modified Tersoff Potential for Pure and Hydrogenated Diamond-like Carbon. *Comput. Mater. Sci.* **2013,** *67*, 146-150.
32. Mo, Y. F.; Turner, K. T.; Szlufarska, I., Friction Laws at the Nanoscale. *Nature* **2009,** *457*, 1116-1119.
33. Jonnalagadda, K. N.; Chasiotis, I., Strength and Fracture Resistance of Amorphous Diamond-like Carbon Films for MEMS. *J. Nanomater.* **2009,** *204281*, 1-8.
34. Jacobs, T. D. B.; Carpick, R. W., Nanoscale Wear as a Stress-assisted Chemical Reaction. *Nat. Nanotechnol.* **2013,** *8* (2), 108-112.
35. Gotsmann, B.; Lantz, M. A., Atomistic Wear in a Single Asperity Sliding Contact. *Phys. Rev. Lett.* **2008,** *101*, 125501.

36. Vargonen, M.; Yang, Y. J.; Huang, L. P.; Shi, Y. F., Molecular Simulation of Tip Wear in a Single Asperity Sliding Contact. *Wear* **2013,** *307*, 150-154.
37. Bowden, F. P.; Tabor, D., Mechanism of Friction and Lubrication in Metal-working. *J. Inst. Pet.* **1954,** *40*, 243-253.

Table of Contents